Generalized source term multiflux method coupled with Runge-Kutta ray tracing technique for arbitrary radiative intensity of graded-index media

Linyang Wei,[1] Hong Qi,[2,*] Guojun Li,[1,†] and Weijun Zhang[1]
[1]*School of Metallurgy, Northeastern University, Shenyang 110819, People's Republic of China*
[2]*School of Energy Science and Engineering, Harbin Institute of Technology, Harbin 150001, People's Republic of China*

(Received 6 October 2020; revised 6 March 2021; accepted 3 May 2021; published 1 June 2021)

The generalized source term multiflux method (GSMFM) combined with Runge-Kutta ray tracing technique is developed to calculate arbitrary directional radiative intensity of graded-index media. In this method, the finite volume method is employed to solve source terms along the curved ray path determined by the Fermat principle. Runge-Kutta ray tracing technique is adopted to obtain the ray trajectory numerical solution in graded-index media. And the GSMFM is used to solve radiative intensity to be expected. One-dimensional and two-dimensional radiative heat transfer problems are investigated to verify the performance of this method. The numerical results show that the accuracy of the GSMFM is close to that of backward Monte Carlo (BMC) method, while the efficiency of GSMFM is much higher than that of the BMC. Therefore, the GSMFM developed can be considered as a promising method to solve arbitrary radiative intensity in graded-index media.

DOI: 10.1103/PhysRevE.103.063301

I. INTRODUCTION

Due to the heterogeneity of composition, density, and temperature distribution of semitransparent media, the refractive index of a media may be a function of spatial position [1,2]. The rays propagating inside the medium with graded refractive index (GRI) are not straight lines, but curved lines determined by the Fermat principle [3]. With the development of relevant technical researches, radiative heat transfer (RHT) in semitransparent media with GRI has attracted considerable attention, and many experts and scholars have begun to carry out related studies. Compared with uniform refractive index (URI), RHT process in semitransparent media with GRI becomes more complicated, which means the solution of RHT would be more difficult. There are two main reasons: (i) the volumetric characteristic and path characteristic of RHT in the participating media; (ii) the light travelling along the curved path in the medium [4,5]. Due to the complexity of RHT process in semitransparent medium with GRI, there is no method can solve this problem perfectly at present. Therefore, how to solve RHT is still a very active field with great demand.

During the last three decades, a considerable effort of investigation has been focused on the RHT in semitransparent with GRI. For instance, Siegel *et al.* [6] took the lead in the study of RHT problems inside the GRI medium in 1993 and analyzed the effects of GRI on RHT in the scattering multilayer regions. After that, Abdallah *et al.* [7,8] done a lot of work on the solution of RHT problems in GRI media, and they developed a curved ray-tracing technique to solve the quasi-steady RHT problems and coupled radiation-conduction problems in the media with GRI. Lemonnier *et al.* [9] derived the formulation of radiative transfer equation (RTE) in both conservative and nonconservative forms with GRI and adopted the discrete ordinates method to solve one-dimensional RHT problems. Xia *et al.* [10] developed a curved Monte Carlo method to solve the RHT in an absorbing and scattering medium with arbitrary refractive index distribution and studied the effects of optical thickness, refractive index distribution and boundary characteristics on temperature and radiative heat flux. Liu *et al.* [11–13] introduced finite element method and discontinuous finite element method to solve steady and transient RHT which avoid the complicated and time-consuming computation of curved ray trajectories. Sarvari *et al.* [14] developed a multigrid Monte Carlo method (MCM) to solve RHT in multidimensional GRI media with diffuse-specular-gray boundaries and comparison with benchmark solutions showed that the method is accurate. Wang *et al.* [15] proposed a modified MCM to solve transient RHT in a one-dimensional scattering medium with GRI and the computational efficiency is improved greatly by introducing time shift and superposition principle. Wu *et al.* [16] adopted integral equation method based on exact ray paths to solve RHT in a slab at radiative equilibrium and in an isothermal slab. Cheng *et al.* [17–20] extended the distributions of ratios of energy scattered or reflected (DRESOR) method to solve the RHT problems in medium with GRI. However, the most methods mentioned above can only obtain integral radiative quantities or several radiative intensities in very limited directions and can't solve arbitrary directional radiative intensity accurately and flexibly, which can't meet requirement of practical engineering [21].

According to the authors' best knowledge, it is rather limited to calculate arbitrary radiative intensity accurately and quickly based on the existing methods, especially for the radiative transfer problems in GRI medium. The backward Monte Carlo (BMC) method based on radiation distribution

*qihong@hit.edu.cn
†ligj@mail.neu.edu.cn

factors [22] can calculate radiative intensity accurately, but time-consuming ray tracing process is unavoidable, especially involving variable properties and complex boundaries. The DRESOR method based on MC model [18] can solve radiative intensity accurately, but MC calculation takes a lot of time and the formulations of DRESOR are complex, especially in complex shape and boundary conditions, which would limit its application. Our groups developed an integral equation method based on radiation distribution factors (RDFIEM) [4] can solve arbitrary radiative intensity in the semitransparent media with GRI. However, the calculation of radiation distribution factors (RDF) database of RDFIEM is very time-consuming and the RDF database need to be recalculated once the physical properties change. Therefore, there is still a substantial requirement to develop efficient and accurate numerical techniques to solve arbitrary radiative intensity of semitransparent media with GRI.

With this idea in mind, the generalized source term multi-flux method (GSMFM) coupled with Runge-Kutta ray tracing (RKRT) technique is developed for arbitrary radiative intensity solution in semitransparent media with GRI in present research. This method takes into account both calculation accuracy and calculation efficiency compared with existing numerical methods. The remaining of this paper is organized in the following sequence. The mathematical theory and comprehensive formulation of the GSMFM for radiative intensity solution in the semitransparent GRI media is given in Sec. II. One-dimensional and two-dimensional cases are investigated to demonstrate the performance of the GSMFM in Sec. III. The main conclusions and remarks are provided in Sec. IV.

II. THEORETICAL MODEL

A. The mathematical expression of GSMFM

As shown in Fig. 1, an arbitrary multidimensional semitransparent medium with GRI is considered. The light ray goes along a curved path determined by the Fermat principle.

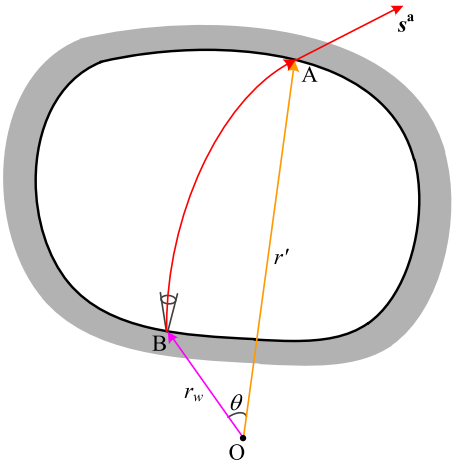

FIG. 1. The physical model of light transmission in medium with GRI.

The corresponding RTE is given by [23]

$$n^2\frac{d}{ds}\left[\frac{I(\mathbf{r},\mathbf{\Omega})}{n^2}\right] = -(\kappa_a+\sigma_s)I(\mathbf{r},\mathbf{\Omega}) + n^2\kappa_a I_b + \frac{\sigma_s}{4\pi}\int_{4\pi} I(\mathbf{r},\mathbf{\Omega}')\,\Phi(\mathbf{\Omega},\mathbf{\Omega}')d\Omega', \quad (1)$$

and the corresponding boundary condition can be directly imposed as follows [24]:

$$I_{\rm w}(\mathbf{\Omega}) = n_w^2\varepsilon_w I_{b,w} + \frac{1-\varepsilon_w}{\pi}\int_{\mathbf{n}_w\cdot\mathbf{\Omega}'<0} I_{\rm w}(\mathbf{\Omega}')|\mathbf{n}_w\cdot\mathbf{\Omega}'|d\mathbf{\Omega}', \quad (2)$$

where I is the radiative intensity; $I_{\rm b}$ is the blackbody radiative intensity; I_w is the radiative intensity at boundary wall; n represents the refractive index; s is the arc length; $\mathbf{r}$ denotes the position vector; $\mathbf{\Omega}$ indicates the direction of radiative intensity; κ_a is the absorption coefficient; $\sigma_{\rm s}$ is the scattering coefficient; Φ means the scattering phase function; π is the circumference rate; ε is the emissivity; $\mathbf{n}_w$ is the unit outer normal vector at boundary wall.

Along the curved ray path, the RTE can be written as

$$\frac{d}{ds}\left[\frac{I(s,\mathbf{\Omega})}{n^2}\right] + (\kappa_a+\sigma_s)\frac{I(s,\mathbf{\Omega})}{n^2} = S(s), \quad (3)$$

where $S(s)$ represents the generalized source item which can be expressed as

$$S(s) = \kappa_a I_b(s) + \frac{\sigma_s}{4\pi}\int_{4\pi}\frac{I(s,\mathbf{\Omega}')}{n^2}\Phi(\mathbf{\Omega}',\mathbf{\Omega})d\Omega'. \quad (4)$$

The integral form of the solution of Eq. (3) can be written as [3]

$$\frac{I(s,\mathbf{\Omega})}{n^2} = \frac{I(s_0,\mathbf{\Omega})}{n_0^2}\exp\left[-\int_{s_0}^{s}(\kappa_a+\sigma_s)ds\right] + \int_{s_0}^{s} S(s')\exp\left[-\int_{s'}^{s}(\kappa_a+\sigma_s)ds\right]ds'. \quad (5)$$

From the above formulations, it can be seen that the key problem is to solve the generalized source term which is the basis of calculating radiative intensity. The Finite volume method (FVM), as a mature and reliable method, is selected to calculate generalized source terms. In the Cartesian

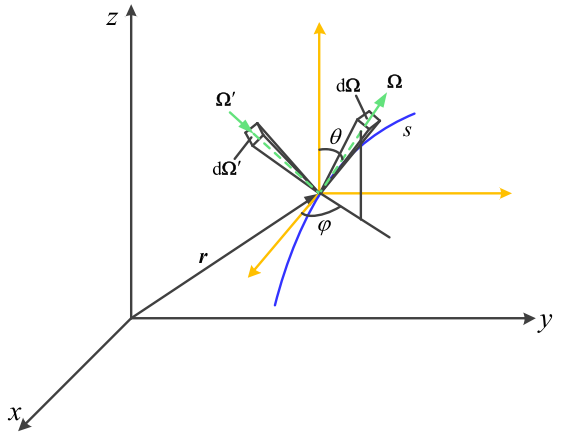

FIG. 2. The physical model in Cartesian coordinate system.

coordinate system shown in Fig. 2, the radiative intensity is a function of variables x, y, z, θ, and φ. The RTE can be expressed in a divergence form as [25]

$$\boldsymbol{\Omega}\cdot\nabla I(\mathbf{r},\Omega)+\frac{1}{2n^2\sin\theta}\frac{\partial}{\partial\theta}\{[I(\mathbf{r},\Omega)(\xi\boldsymbol{\Omega}-\boldsymbol{k})]\cdot\nabla n^2\}+\frac{1}{2n^2\sin\theta}\frac{\partial}{\partial\varphi}\{I(\mathbf{r},\boldsymbol{\Omega})[\boldsymbol{s}_1\cdot\nabla n^2]\}+(\kappa_a+\sigma_s)I(\mathbf{r},\Omega)$$
$$=n^2\kappa_a I_b+\frac{\sigma_s}{4\pi}\int_{4\pi}I(\mathbf{r},\Omega')\Phi(\Omega,\Omega')d\Omega', \tag{6}$$

where

$$\boldsymbol{\Omega}=\boldsymbol{i}\mu+\boldsymbol{j}\eta+\boldsymbol{k}\xi=\boldsymbol{i}\sin\theta\cos\varphi+\boldsymbol{j}\sin\theta\sin\varphi+\boldsymbol{k}\cos\theta, \tag{7a}$$

$$\boldsymbol{s}_1=-\boldsymbol{i}\sin\varphi+\boldsymbol{j}\cos\varphi. \tag{7b}$$

The piecewise constant angular quadrature is employed to treat the two angular redistribution terms of Eq. (6). One appropriate closure relation based on the step schemes (setting the downstream surface intensities equal to the upstream center intensities) is selected to treat the relation between the intensities on the cell surfaces and the cell center intensities. The final discretized equation of RTE in a three-dimensional medium with GRI can be expressed as [25]

$$\left[\sum_{i=1}^{N_p}\frac{n_i^2}{n_p^2}\max\left(A_iD_i^{m,n},0\right)+\max\left(\chi_\theta^{m+\frac{1}{2},n},0\right)+\max\left(-\chi_\theta^{m-\frac{1}{2},n},0\right)+\max\left(\chi_\varphi^{m,n+\frac{1}{2}},0\right)+\max\left(-\chi_\varphi^{m,n-\frac{1}{2}},0\right)\right.$$
$$\left.+\Delta V_p\Delta\Omega^{m,n}(\kappa_{a,p}+\sigma_{s,p})-\Delta V_p\Delta\Omega^{m,n}\frac{\sigma_{s,p}}{4\pi}\bar{\Phi}_p^{m,n;m,n}\Delta\Omega^{m,n}\right]I_p^{m,n}$$
$$=\sum_{i=1}^{N_p}\frac{n_i^2}{n_{p_i}^2}\max\left(-A_iD_i^{m,n},0\right)I_{p_i}^{m,n}+\max\left(-\chi_\theta^{m+\frac{1}{2},n},0\right)I_p^{m+1,n}+\max\left(\chi_\theta^{m-\frac{1}{2},n},0\right)I_p^{m-1,n}+\max\left(-\chi_\varphi^{m,n+\frac{1}{2}},0\right)I_p^{m,n+1}$$
$$+\max\left(\chi_\varphi^{m,n-\frac{1}{2}},0\right)I_p^{m,n-1}\Delta V_p\Delta\Omega^{m,n}n_p^2\kappa_{a,p}I_{b,p}+\Delta V_p\Delta\Omega^{m,n}\frac{\sigma_{s,p}}{4\pi}\times\sum_{m',n';m'\neq m,n'\neq n}I_p^{m',n'}\bar{\Phi}_p^{m',n';m,n}\Delta\Omega^{m',n'}. \tag{8}$$

where n_i is the refractive index at the ith surface; n_p is the refractive index of ith cell; A_i is the surface area of cell; D_i is the direction cosine integrated over control solid angle; χ_θ and χ_φ are the coefficients of the discretization equation; ΔV is the volume of control volume; $\Delta\Omega$ is the control solid angle; $\bar{\Phi}$ is the averaged scattering phase function. This is a general finite volume formulation of RTE in arbitrary three-dimensional medium with GRI. It is applicable for any type of volume cell shape (structured or unstructured). Equation (8) is employed to calculate the incident radiative intensity of source terms as shown in Eq. (4), and then the numerical integration of the source term can be discretized as

$$S(s)=\kappa_aI_b(s)+\frac{\sigma_s}{4\pi}\sum_{i=1}^{NL}\frac{I(s,\Omega^i)}{n_s^2}\Phi\left(\Omega^i,\Omega\right)\Delta\Omega^i, \tag{9}$$

where NL is the number of discrete directions. The final mathematical formulation of GSMFM can be described as follows:

$$\frac{I_i^{\mathrm{a}}}{n_i^2}=\frac{I_{i-1}^{\mathrm{a}}}{n_{i-1}^2}\exp\left[-(\kappa_{a,i}+\sigma_{s,i})\Delta s_i\right]+\frac{S_i}{(\kappa_{a,i}+\sigma_{s,i})}$$
$$\times\{1-\exp\left[-(\kappa_{a,i}+\sigma_{s,i})\Delta s_i\right]\},\qquad i=1,\ldots,N, \tag{10}$$

where Δs_i is arc length between adjacent nodes. It should be noted that the computational speed and accuracy of the GSMFM would be slightly lower than those of FVM. This is because GSMFM is based on the FVM which is employed to solve source terms. The GSMFM includes source term calculation and integral calculation, which causes GSMFM have a little larger numerical error and take a little more time than FVM.

Another problem is the determination of integral path (i.e., the solution of ray path). The rays propagating inside the medium with GRI are curved lines determined by the Fermat principle. Unfortunately, the analytical solution of ray trajectory can't be obtained in most cases. The numerical solution of ray trajectory is usually employed to describe the light transmission. The detailed description of a numerical calculation of the ray tracing would be given in the next section.

B. Ray tracing procedure

In gradient index media, the refractive index is a function of spatial coordinates. The Fermat principle holds that the optical path of an actual ray between any two points is shorter than that of any curve connecting the two points. The corresponding ray equation is

$$\frac{d}{ds}\left[n(\boldsymbol{r})\frac{d\boldsymbol{r}}{ds}\right]=\mathrm{grad}n(\boldsymbol{r}), \tag{11}$$

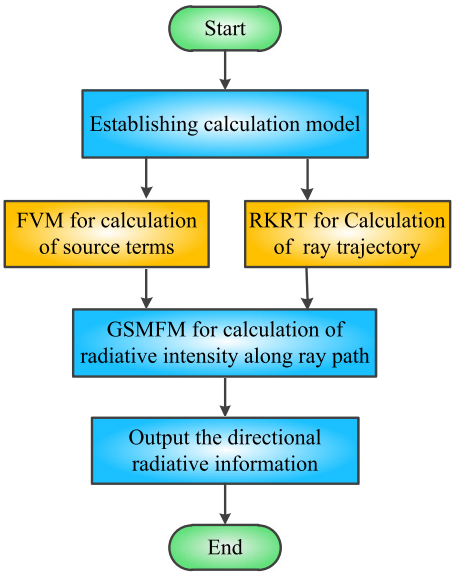

FIG. 3. The flowchart of GSMFM for calculating radiative intensity.

where $n(\boldsymbol{r})$ is a function of coordinates, not the arc length s; grad is gradient operator.

The Runge-Kutta ray tracing (RKRT) method is used to calculate ray trajectory. The RKRT ray tracing technique was developed by Sharma *et al.* [26,27] in 1980s. This method is widely used because of its high precision and simple calculation. First, the position matrix **R** and ray vector **T** is introduced here [28],

$$\mathbf{R} = [x, y, z]^{\mathrm{T}}, \tag{12}$$

$$\boldsymbol{T} = \frac{d\boldsymbol{r}}{dt} = n(\boldsymbol{r})\frac{d\boldsymbol{r}}{ds} = n(\boldsymbol{r})[\mu,\ \eta,\ \xi]^{\mathrm{T}}, \tag{13}$$

where μ, η, ξ are the cosine values of the ray vector respecting to the x, y, and z axis, respectively; t is a new variable that is

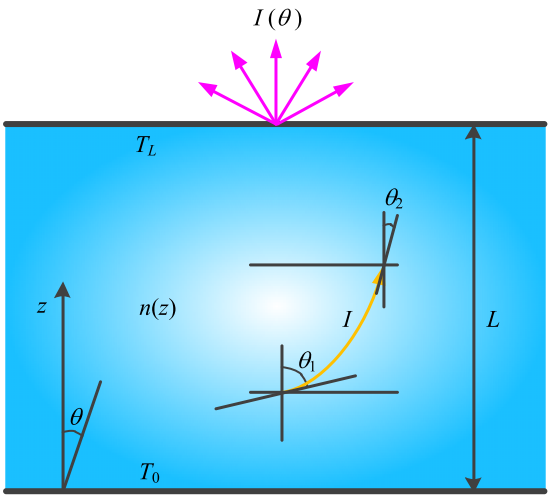

FIG. 4. Physical geometry of one-dimensional slab medium.

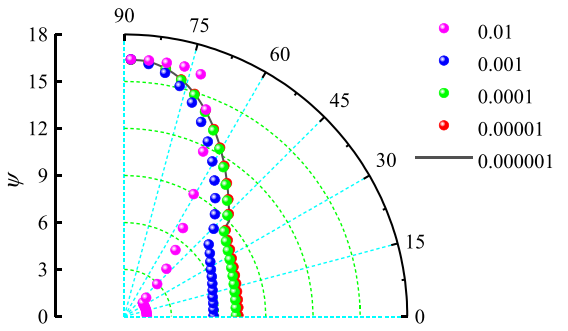

FIG. 5. The radiative intensity with different step sizes of Runge-Kutta ray tracing.

defined as [28]

$$t = \int \frac{ds}{n(\boldsymbol{r})}. \tag{14}$$

Then, the matrix **D** is defined as [28]

$$\mathbf{D} = n(\boldsymbol{r})\nabla n(\boldsymbol{r}) = \frac{1}{2}\nabla n(\boldsymbol{r})^2 = \frac{1}{2}\left[\frac{\partial n^2}{\partial x}, \frac{\partial n^2}{\partial y}, \frac{\partial n^2}{\partial z}\right]^{\mathrm{T}}. \tag{15}$$

Finally, the standard ordinary differential equation is obtained as follows [28]:

$$\mathbf{T}' = \mathbf{D}. \tag{16}$$

The Runge-Kutta formulas are employed to calculate the **R** and **T**, and they can be expressed as [28]

$$\begin{aligned} k_1 &= \Delta t D(R_n), \\ k_2 &= \Delta t D(R_n + \Delta t/2 T_n + \Delta t/8 k_1), \\ k_3 &= \Delta t D(R_n + \Delta t T_n + \Delta t/2 k_2), \end{aligned} \tag{17}$$

$$\begin{aligned} R_{n+1} &= R_n + \Delta t/6(6T_n + k_1 + 2k_2), \\ T_{n+1} &= T_n + 1/6(k_1 + 4k_2 + k_3), \end{aligned} \tag{18}$$

where Δt is the step size, indicating the increment of t; $k = 1$, $k = 2$, and $k = 3$ are the intermediate variables. The ray trajectory in semitransparent media with GRI can be obtained by using Eqs. (17) and (18).

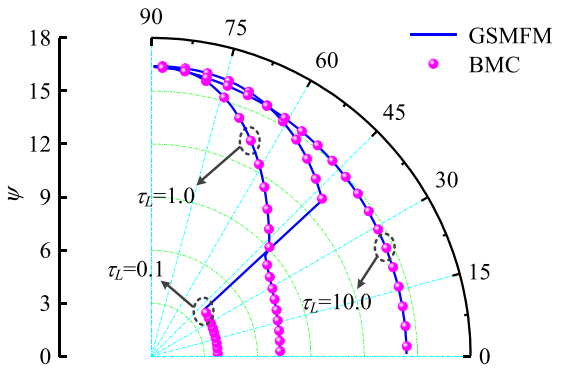

FIG. 6. The radiative intensity of different optical thicknesses.

TABLE I. The average calculation time of BMC and GSMFM for each radiative intensity.

Method	Time for $\tau_L = 0.1$	Time for $\tau_L = 1$	Time for $\tau_L = 10$
BMC	9.765×10^{-2} s	1.406×10^{-1} s	1.410×10^{-1} s
GSMFM	1.444×10^{-3} s	1.722×10^{-3} s	1.667×10^{-3} s

III. SOLUTION AND DISCUSSION

The mathematical theory of radiative intensity and ray trajectory calculation has been given in the last section. To better show the whole calculation process, a flowchart of GSMFM is illustrated in Fig. 3. In this section, various cases (including one-dimensional and two-dimensional radiation problems) are investigated to demonstrate the performance of GSMFM and all the calculations run on an Intel Core i7-3770 PC with a Pentium (R) D (3.40 GHz)CPU with 16.0 GB RAM.

A. Solution of one-dimensional RHT problems

1. Radiation calculation in pure absorbing medium

As shown in Fig. 4, one-dimensional slab with GRI is considered. In this case, the slab is assumed to be a pure absorbing medium with thickness L. The upper and lower boundaries are opaque, diffuse, and gray walls whose emissivities are ε_0 and ε_L, respectively. The temperatures of the bounding walls are T_0 and T_L, and the temperature of medium between the boundary walls varies with the coordinate z. The absorption coefficient κ_a is uniform over the slab. The refractive index distribution within the medium is set as

$$n(z) = 1.2 + 0.6(z/L). \tag{19}$$

The GSMFM is applied to solve this one-dimensional problem in which the temperature of medium between the boundary walls varies from T_0 to T_L linearly. The radiative intensity (dimensionless form expressed as $\psi = \pi I/\sigma T_0^4$) at the center of the upper boundary is calculated. Here, the effects of step size of Runge-Kutta ray tracing on calculation results of radiative intensity are analyzed first. Because the stability of the GSMFM mainly depends on the discretization error which is determined by the step size of Runge-Kutta ray tracing in numerical integration. The optical thickness is set as $\tau_L = 1$ and the wall temperature are set as $T_0 = 1000$ K and $T_L = 1500$ K, respectively. The calculation results of radiative intensity are shown in Fig. 5 from which it can be seen that step size has an important influence on calculation results of GSMFM. When the step size of Runge-Kutta ray tracing is too large (such as $\Delta t = 0.01$), there is a serious deviation in the calculation results. With the decrease of step size, the calculation results tend to be stable. When the step size is reduced to 0.00001, the calculation results of GSMFM are almost unchanged. In other words, the influence of discretization error can be ignored and the calculation result is stable when the step size is small enough. Therefore, the step size $\Delta t = 0.00001$ is adopted in the following cases.

The calculation results for different optical thicknesses are shown in Fig. 6 from which it can be seen a perfect agreement between GSMFM and BMC, and the maximum relative error is only 0.18%. This observation shows that the accuracy of GSMFM is very close to the BMC. It can be also noted that there is a "jump" behavior of a continue line. There are two main reasons for this observation: (1) temperature profiles and (2) refractive index profiles. Because the ray propagates along the curve determined by Fermat principle in gradient index medium, there is a critical zenith angle θ_{cr} which causes a "jump" in the radiative intensity profile. When the zenith angle $\theta < \theta_{cr}$, the starting point of the integral path lies in the lower boundary whose temperature is 1000 K. When the zenith angle $\theta > \theta_{cr}$, the starting point of the integral path

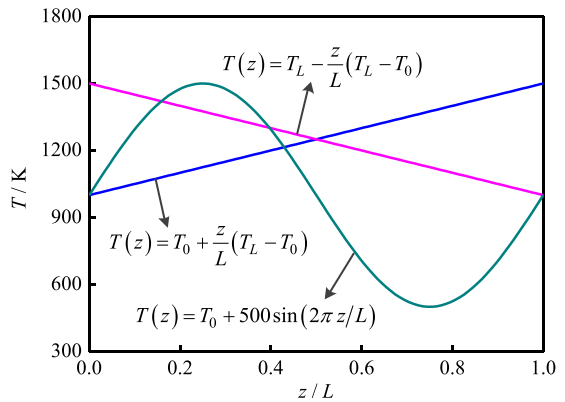

FIG. 7. The temperature distributions in semitransparent medium with GRI.

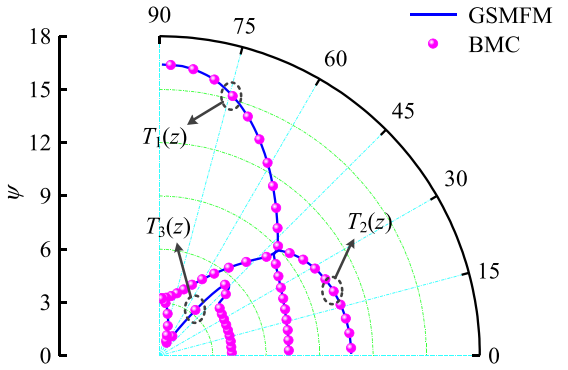

FIG. 8. The radiative intensity of different temperature distributions.

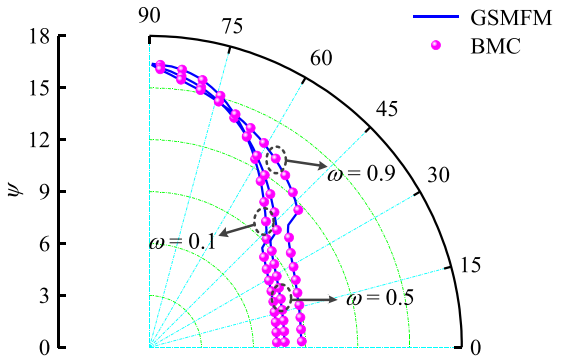

FIG. 9. The radiative intensity of different scattering albedos.

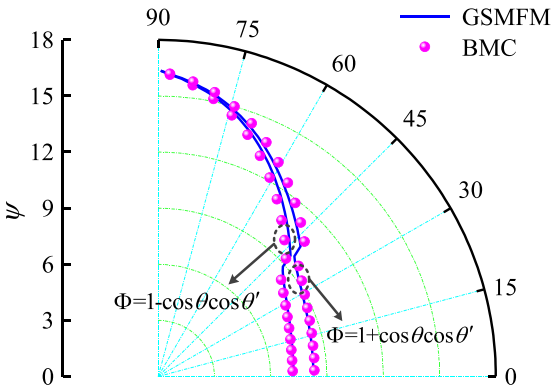

FIG. 10. The radiative intensity for anisotropic scattering medium.

lies in the upper boundary due to the total reflection, and temperature of upper boundary is 1500 K. Therefore, there is a jump in the radiative intensity profile. Moreover, the smaller the optical thickness, the more obvious this phenomenon is. Because the smaller the optical thickness, the greater the contribution of the boundary to the radiative intensity. The calculation time is different as shown in Table I. The calculation time of BMC (the ray number is selected as 10^6) is nearly two orders of magnitude longer than that of GSMFM (including the time of FVM for calculating generalized source term). Therefore, the precision of GSMFM is very close to that of BMC, and the efficiency is much higher than that of BMC.

Not only the optical thickness but also the temperature distribution affects the radiative intensity. Three temperature distributions as shown in Fig. 7 are selected and optical thickness is set as $\tau_L = 1$. The calculated results of radiative intensity are presented in Fig. 8. It can be seen that temperature distribution has a large effect on radiative intensity. Radiative intensity increases with increasing of zenith angle for linear increasing temperature distribution within medium [namely, $T_1(z)$], while radiative intensity decreases with increasing of zenith angle for linear decreasing temperature distribution within medium [namely, $T_2(z)$]. There are peak and trough in radiative intensity distribution for sinusoidal temperature distribution within medium [namely, $T_3(z)$]. All

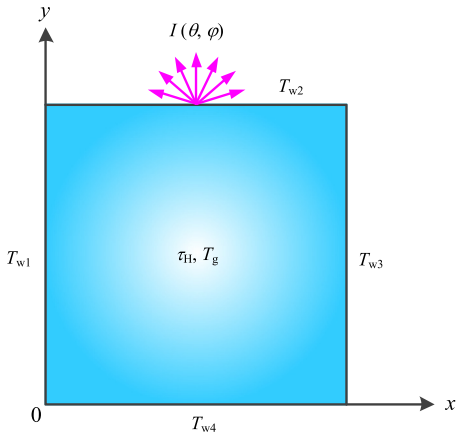

FIG. 11. Physical geometry of two-dimensional medium with GRI.

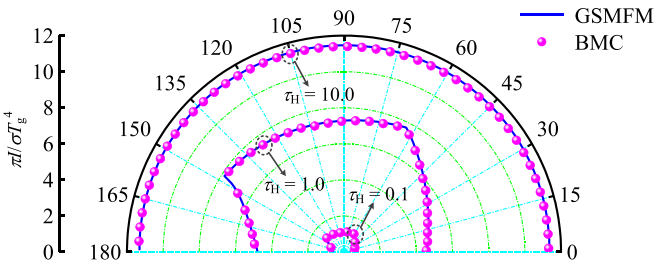

FIG. 12. The radiative intensity of different optical thicknesses.

simulated results of GSMFM agree with those of BMC, which shows the GSMFM we developed is accurate.

2. Radiation calculation in absorbing-emitting-scattering medium

The scattering of medium would change the direction of thermal ray propagation, which makes the radiative transfer process more complicated. The calculation of RHT in absorbing-emitting-scattering medium with GRI is difficult but necessary. Therefore, radiation calculation in absorbing-emitting-scattering medium is studied in this section. The physical model as shown in Fig. 4, the optical thickness is set as $\tau_L = 1$, the temperature of medium between the boundary walls varies form $T_0 = 1000$ K to $T_L = 1500$ K linearly, and wall emissivity of the both boundaries are set as $\varepsilon_0 = \varepsilon_L = 1$. Figure 9 gives the simulation results for different scattering albedos and it can be observed that radiative intensity calculated by GSMFM are consistent with those of BMC, and the maximum relative error is 0.56% for $\omega = 0.1$, 0.52% for $\omega = 0.5$ and 0.76% for $\omega = 0.9$, respectively. This proves that the GSMFM is very accurate, even if the scattering characteristics of the medium are considered.

In this case, the anisotropic scattering medium with single scattering albedo $\omega = 0.5$ is studied by the GSMFM and the other parameters including GRI, optical thickness, wall emissivity and temperature distribution are the same as those of the last case. The scattering phase function is assumed to be $\Phi = 1 + b\cos\theta\cos\theta'$ ($b = 1$ represents forward scattering and $b = -1$ represents forward scattering). The calculation results are shown in Fig. 10 from which it can be seen that the results obtained by the GSMFM agree with those of BMC very well, and the maximum relative error is less than 3.17%. This observation indicates that the GSMFM is accurate for solving the radiative transfer in anisotropic scattering media. Figures 9 and 10 show that scattering characteristic has a significant influence on radiative transfer and the GSMFM is a promising numerical method to solve arbitrary radiative intensity in absorbing-emitting-scattering medium with GRI.

TABLE II. The average calculation time for different optical thicknesses.

Method	Time for $\tau_L = 0.1$	Time for $\tau_L = 1$	Time for $\tau_L = 10$
BMC	1.598 s	1.221 s	0.352 s
GSMFM	4.744×10^{-2} s	4.763×10^{-2} s	4.192×10^{-2} s

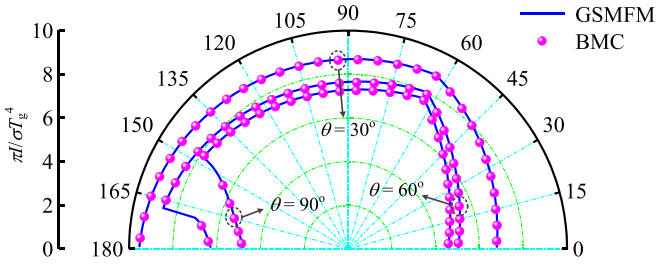

FIG. 13. The radiative intensity along different zenith angles.

B. Solution of two-dimensional RHT problems

1. Radiation calculation in pure absorbing medium

In this section, two-dimensional RHT problems in semi-transparent medium with GRI are studied. The physical model is shown in Fig. 11. The cross-sectional area of the media is $L_x \times L_y$, the medium is assumed to be gray and the four boundaries are blackbody wall with temperature T_{w1}, T_{w2}, T_{w3}, and T_{w4}. The radial refractive index distribution is adopted and can be expressed as

$$n(x, y) = n_{\text{ref}}[1 - a^2(x^2 + y^2)/H^2]^{0.5}, \tag{20}$$

where $n_{\text{ref}} = 5$ and $a = 0.66$.

The radiative intensity at the center of top boundary is calculated as shown in Fig. 11. The medium is assumed to be pure absorbing medium, the temperature of medium is set as $T_{\text{g}} = 1000$ K, and the four boundaries are assumed to be cold boundaries (namely, $T_{w1} = T_{w2} = T_{w3} = T_{w4} = 0$ K). Figure 12 gives the radiative intensity distribution ($\theta = 90°$) for different optical thickness. It can be seen that the results of the GSMFM agree with those of BMC very well and the maximum relative error is only 0.15% for $\tau_H = 0.1$, 0.25% for $\tau_{\text{H}} = 1$, and 0.72% for $\tau_{\text{H}} = 10$, respectively. The computational time are shown in Table II from which it can be found that the time of GSMFM is far less than that of BMC. This observation indicates that the GSMFM we developed not only has high precision, but also has high efficiency. Figure 13 shows radiative intensity distribution along different zenith angles ($\theta = 30°$, $60°$, and $90°$) in which the optical thickness is $\tau_{\text{H}} = 1$. It can be observed that radiative intensity distributions are similar. And for the same circumferential angle, the larger the zenith angle is, the smaller the radiative intensity is.

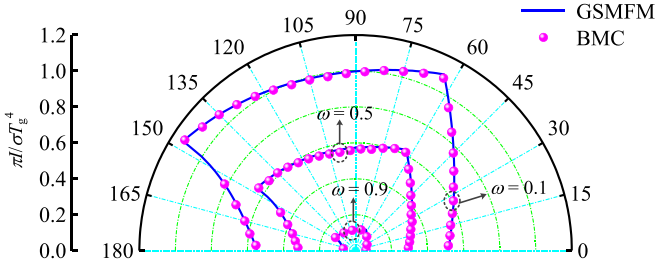

FIG. 14. The radiative intensity of different scattering albedos.

TABLE III. The average calculation time for different scattering albedos.

Method	Time for $\omega = 0.1$	Time for $\omega = 0.5$	Time for $\omega = 0.9$
BMC	1.600 s	1.627 s	1.837 s
GSMFM	6.556×10^{-2} s	9.033×10^{-2} s	8.002×10^{-2} s

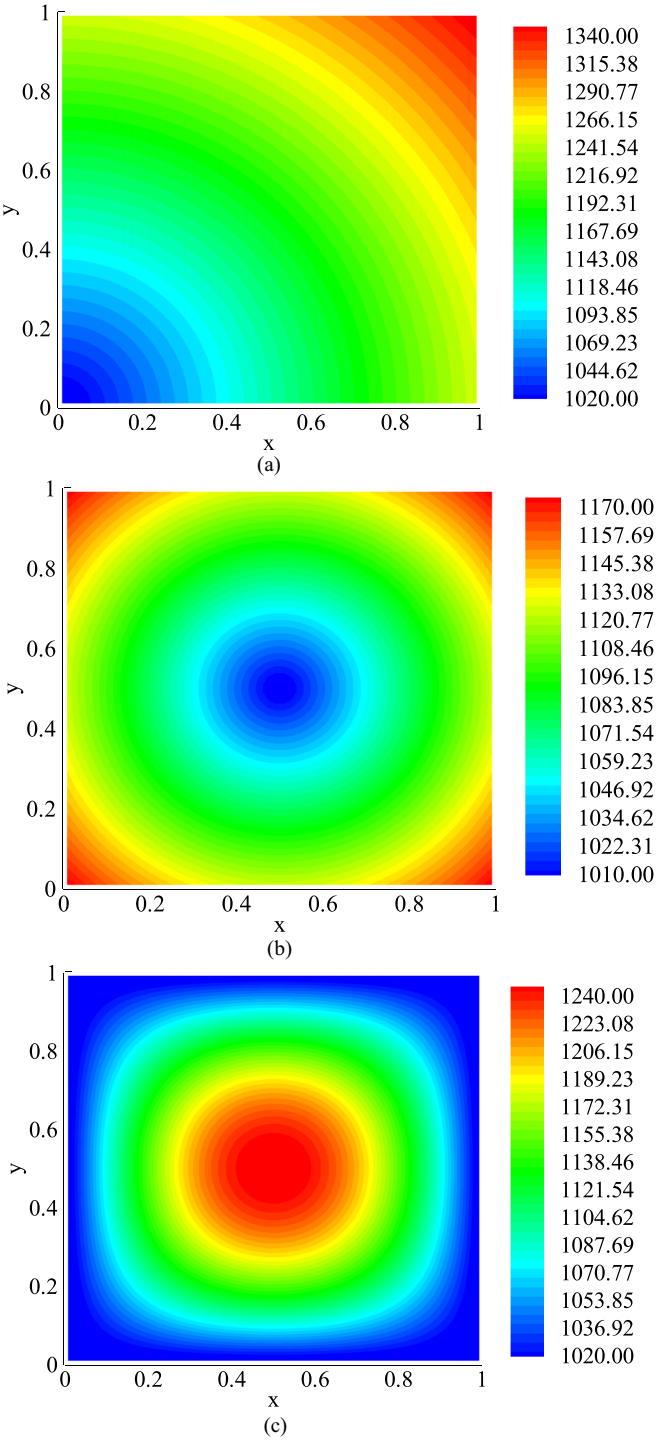

FIG. 15. Temperature distributions: (a) $T = T_g + \frac{T_g}{4}\sqrt{(x/H)^2 + (y/H)^2}$, (b) $T = T_g + \frac{T_g}{4}\sqrt{(\frac{x}{H} - \frac{1}{2})^2 + (\frac{y}{H} - \frac{1}{2})^2}$, and (c) $T = T_g + \frac{T_g}{4}\sin(\frac{\pi x}{H})\cos(\frac{\pi y}{H} - \frac{1}{2})$.

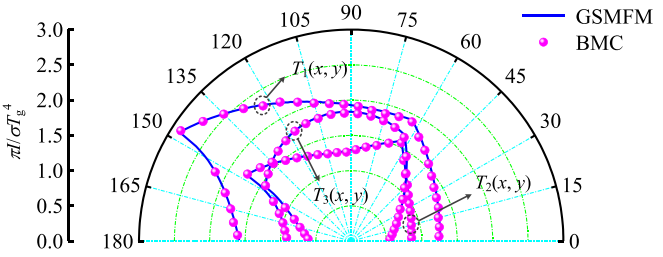

FIG. 16. The radiative intensity of different temperature distributions.

2. *Radiation calculation in absorbing-emitting-scattering medium*

The absorbing-emitting-scattering medium with GRI is investigated in this case and the physical model is the same as the last case. The optical thickness is set as $\tau_H = 0.1$, isotropic scattering is selected, and the other parameters are the same as those of last case. Figure 14 shows the calculated radiative intensity for different scattering albedos. No observable difference could be observed between the results of the GSMFM and BMC, which proves that scattering characteristic has no effect on the accuracy of the GSMFM. The computational time for different scattering albedos are shown in Table III from which it can be found that the time of GSMFM is far less than that of BMC. This observation indicates that the GSMFM we developed take high precision and high efficiency into account. It can be also noted that scattering albedo has a remarkable effect on the radiative intensity distribution. With the increase of scattering, the radiative intensity distribution becomes more uniform. Thus, scattering characteristic of medium is an important factor for RHT and it is necessary to study radiative intensity calculation in absorbing-emitting-scattering medium with GRI. Another case considers effect of temperature distribution on radiative transfer. The optical thickness is set as $\tau_H = 0.1$, the single scattering albedo is $\omega = 0.1$, and other parameter settings remain the same. Three different temperature distributions as shown in Fig. 15 are selected and the corresponding radiative intensity distribution is shown in Fig. 16. Comparison of calculated results between GSMFM and BMC shows that GSMFM is a promising numerical method with high accuracy.

IV. CONCLUSIONS

The GSMFM combined with Runge-Kutta ray tracing technique is developed to calculate arbitrary directional radiative intensity of graded-index media. The FVM as a preprocessing method to solve the source terms simplifies the integration process of the RTE, and the GSMFM is employed to solve arbitrary directional radiative intensity. Hence, the main advantage of GSMFM is to get rid of angle discretization and break through the limitation of fixed direction discretization schemes. One-dimensional and two-dimensional cases show that the accuracy of the GSMFM is very close to that of BMC, while the efficiency is higher than that of BMC. The optical thickness and single scattering albedo have almost little effects on the accuracy of the GSMFM. And temperature distribution has a significant effect on radiative intensity. Therefore, the GSMFM developed can be considered as a promising numerical method in various radiative research fields. Further study will focus on extending the method to the computation of RHT in nongray media in the practical engineering applications.

ACKNOWLEDGMENTS

The support of this work by the China Postdoctoral Science Foundation (Grant No. 2020M680968), National Key Research and Development Program of China (Grant No. 2017YFA0700300), the National Natural Science Foundation of China (Grant No. U1760115), and the National Natural Science Foundation of China (Grant No. 51976044) are gratefully acknowledged. A very special acknowledgment is also made to the editors and referees who made important comments to improve this paper.

[1] L. H. Liu, J. Quant. Spectrosc. Radiat. Transfer **102**, 293 (2006).
[2] J. M. Zhao and L. H. Liu, Int. J. Heat Mass Transfer **50**, 2634 (2007).
[3] Y. Huang, X. L. Xia, and H. P. Tan, J. Quant. Spectrosc. Radiat. Transfer **74**, 217 (2002).
[4] M. F. Modest, *Radiative Heat Transfer* (Academic Press, San Diego, 2003).
[5] S. M. H. Sarvari, J. Quant. Spectrosc. Radiat. Transfer **199**, 36 (2017).
[6] R. Siegel and C. M. Spuckler, J. Thermophys. Heat Transfer **7**, 624 (1993).
[7] P. B. Abdallah and V. L. Dez, J. Quant. Spectrosc. Radiat. Transfer **65**, 595 (2000).
[8] P. Ben Abdallah and V. Le Dez, J. Quant. Spectrosc. Radiat. Transfer **67**, 125 (2000).
[9] D. Lemonnier and V. L. Dez, J. Quant. Spectrosc. Radiat. Transfer **73**, 195 (2002).
[10] X. L. Xia, D. P. Ren, and H. P. Tan, Numer. Heat Transfer, Part B **50**, 181 (2006).
[11] L. H. Liu, Int. J. Heat Mass Transfer **48**, 2260 (2005).
[12] L. H. Liu, J. Quant. Spectrosc. Radiat. Transfer **103**, 536 (2007).
[13] L. H. Liu and L. J. Liu, Trans. ASME: J. Heat Transfer **129**, 1069 (2007).
[14] S. M. H. Sarvari, J. Quant. Spectrosc. Radiat. Transfer **219**, 61 (2018).
[15] C. H. Wang, Q. Ai, H. L. Yi, and H. P. Tan, Numer. Heat Transfer, Part A **67**, 1232 (2015).
[16] C. Y. Wu and M. F. Hou, Int. J. Heat Mass Transfer **55**, 6600 (2012).
[17] Z. C. Wang, Q. Cheng, G. H. Wang, and H. C. Zhou, J. Quant. Spectrosc. Radiat. Transfer **112**, 2835 (2011).
[18] Z. C. Wang, Q. Cheng, and H. C. Zhou, Int. J. Therm. Sci. **68**, 127 (2013).
[19] Q. Cheng, X. Zhang, Z. F. Huang, Z. C. Wang, and H. C. Zhou, J. Quant. Spectrosc. Radiat. Transfer **143**, 16 (2014).

[20] J. L. Chai, Q. Cheng, J. L. Song, Z. C. Wang, and H. C. Zhou, Int. J. Therm. Sci. **91**, 96 (2015).
[21] Z. Huang, Q. Cheng, and C. Lou, Int. J. Heat Mass Transf. **117**, 296 (2018).
[22] L. H. Liu, J. Thermophys. Heat Transfer **18**, 151 (2003).
[23] L. H. Liu, L. Zhang, and H. P. Tan, J. Quant. Spectrosc. Radiat. Transfer **97**, 436 (2006).
[24] L. H. Liu, J. Thermophys. Heat Transfer **18**, 410 (2003).
[25] L. H. Liu, J. Thermophys. Heat Transfer **20**, 59 (2006).
[26] A. Sharma, D. V. Kumar, and A. K. Ghatak, Appl. Opt. **21**, 984 (1982).
[27] A. Sharma, Appl. Opt. **24**, 4367 (1986).
[28] Y. Huang, G. D. Shi, and K. Y. Zhu, J. Quant. Spectrosc. Radiat. Transfer **176**, 24 (2016).